Physica B 479 (2015) 159–164

Contents lists available at ScienceDirect

Physica B

journal homepage: www.elsevier.com/locate/physb

Two-photon, three-photon, and four-photon excellent near-infrared quantum cutting luminescence of Tm^{3+} ion activator emerged in Tm^{3+}:$YNbO_4$ powder phosphor one material simultaneously

Xiaobo Chen [a,*], Gregory J. Salamo [b], Song Li [a], Jieliang Wang [a], Yuying Guo [a], Yan Gao [c], Lizhu He [d,e], Hui Ma [a], Jingfu Tao [a], Ping Sun [a], Wei Lin [a], Quanlin Liu [d,e]

[a] Department of Physics and Applied Optics Beijing Area Major Laboratory, Beijing Normal University, Beijing 100875, China
[b] Department of Physics, University of Arkansas, Fayetteville, AR 72701, USA
[c] Laboratory of Nanomaterials, National Center for Nanoscience and Technology of China, Beijing 100190, China
[d] School of Materials Science and Engineering, University of Science and Technology Beijing, Beijing 100083, China
[e] State Key Laboratory for Advanced Metals and Materials, University of Science and Technology Beijing, Beijing 100083, China

ARTICLE INFO

Article history:
Received 25 August 2015
Received in revised form
5 October 2015
Accepted 6 October 2015
Available online 13 October 2015

Keywords:
Near-infrared quantum cutting
Luminescence intensity enhancement
$YNbO_4$ powder phosphor
Energy transfer
Tm^{3+} ion
Solar cell

ABSTRACT

In present study, two-photon, three-photon, and four photon near-infrared quantum cutting luminescence of Tm^{3+} ion activator in $YNbO_4$ powder phosphor is reported. The visible to near-infrared excitation and emission spectra and fluorescence lifetimes of $Tm_{0.038}Y_{0.962}NbO_4$ powder phosphor are measured. $Tm_{0.038}Y_{0.962}NbO_4$ is found to possess intense two-photon, strong three-photon, and moderate four-photon quantum cutting 1820 nm $^3F_4 \rightarrow {}^3H_6$ luminescence of the Tm^{3+} ion simultaneously. The up-limit of the two-, three-, and four-photon near-infrared quantum cutting efficiency are found to be approximately 166%, 198%, and 192%, respectively. These results are expected to be valuable in aiding the probing of new generation environmentally friendly germanium Ge solar cells, currently a popular condensed matter physical topic globally.

1. Introduction

Sustainable energy production based on the direct conversion of solar energy is becoming increasingly important as it may be the only source capable of supplying sufficient energy for long-term worldwide energy requirements [1,2]. Quantum cutting materials with quantum efficiency obviously higher than 100% have attracted great interest for their potential applications in solar cells [1–12]. Since the visible quantum cutting luminescence phenomena in Eu^{3+}–Gd^{3+} material was reported by Meijerink et al. in Science [3], the importance, application and significance of the quantum cutting have been widely recognized [1–25]. Although the solar spectrum ranges from 280 nm to 2500 nm at AM 1.5 G [15], the efficiency of normal single junction silicon solar cells is limited to 30% of the Schockley–Queisser limit. More than 70% loss is caused by spectral mismatch losses of transmission and thermalization loss. In 2002, Green et al. proposed the two-photon quantum cutting solar cell theory for the first time, and found that the maximum efficiency of two-photon quantum cutting silicon solar cells can reach 39.6% [10], which are sensitive to the wavelength range 280–1100 nm. Meijerink et al. reported the first experiment phenomena work for second-order near-infrared quantum cutting luminescence in $Yb_xY_{1-x}PO_4$:Tb^{3+} phosphor in 2005 [1]. From 2007, Meijerink [1,15,21], Qiu and Zhou [17], Wang and Chen [5,6], Huang, and Zhang [7], etc. [9,11,23] have reported about 200 literatures of experimental researches of two-photon second-order near-infrared quantum cutting of Sentitizer-Yb^{3+} ion codoped materials, which is used to develop two-photon quantum cutting silicon solar cells [16,19,20]. Qiu and Zhou [2,12], Zhang and Huang [14], our group [8,25] have reported experimental researches of multi-photon first-order near-infrared quantum cutting of Tm^{3+} or Er^{3+} ion activator doped materials from 2009. This further improvement is the multi-photon quantum cutting germanium Ge or silicon-germanium Si–Ge solar cell [2,8,12,14,25], which is sensitive to wavelengths of 280–1850 nm or 280 to about 1650 nm and is environmentally friendly. Its maximum efficiency is able to greatly exceed 39.6% [22] using multi-photon infrared quantum cutting to largely reduce transmission and thermalization losses because the energy band-gap,

* Corresponding author. Fax: +86 10 58800076.
E-mail address: chen78xb@sina.com (X. Chen).

http://dx.doi.org/10.1016/j.physb.2015.10.009

E_g, of Ge is positioned at about 1850 nm (0.67 eV:300 K) [2,8,12,14,25]. Above works are very significant. The present study reports the two-photon, three-photon, and four-photon near-infrared quantum cutting luminescence phenomena in Tm^{3+} ion doped $YNbO_4$ phosphor material. To the knowledge of the authors, this is the first time to find that the effective two-photon, three-photon, and four-photon near infrared quantum cutting are emerged in one material simultaneously. The Tm^{3+} ion is a new attractive near-infrared quantum cutting activator because its quantum cutting process is first-order. This property is useful because, as Meijerink et al. have pointed out [2,8,12,14,25], first-order energy transfer mechanisms generally have a much higher probability (typically a factor of 1000) of occurring than second-order mechanisms. However, so far there have only been ten reports regarding the near-infrared quantum cutting of the about 1800 nm luminescence of the Tm^{3+} activator center [8,14]. Therefore, more thorough study of multi-photon infrared quantum cutting luminescence of Tm^{3+} ion activator is urgently required.

2. Experiment instrument and the sample

The samples used in our experiment were (A) $Tm_{0.005}Y_{0.995}NbO_4$ and (B) $Tm_{0.038}Y_{0.962}NbO_4$ powder phosphors, which were prepared through a solid-state reaction. The starting materials were high-purity Y_2O_3 (99.99%), Nb_2O_5 (99.99%), and Tm_2O_3 (99.99%). The raw powders were weighed according to the stoichiometric compositions and then mixed, ground, and pressed into pellets. Finally, the powders were sintered at 1400 °C for 5 h in a furnace in air. A FL3-2iHR fluorescence spectrometer (Horiba-JY Co., America, Japan, and France) was used to investigate the luminescence of the phosphor powders.

3. The excitation spectra and luminescence spectra and lifetime

First, the visible excitation spectra of 802.5 nm received wavelength of (A) $Tm_{0.005}Y_{0.995}NbO_4$ and (B) $Tm_{0.038}Y_{0.962}NbO_4$ powder phosphors in the wavelength range of 250–710 nm were measured, as shown in part (1) of Fig. 1. The Tm^{3+}:$YNbO_4$ powder phosphor was found to exhibit three groups of excitation spectra signal peaks from ultraviolet to visible. It is found that their main peaks were positioned at 356.5, 461.0 and 682.5 nm. These are easily recognizable as the $^3H_6 \rightarrow {}^1D_2$, $^3H_6 \rightarrow {}^1G_4$, and $^3H_6 \rightarrow {}^3F_3$ absorption transitions, respectively, of the Tm^{3+} ion [12–18].

The excitation spectra of 1820.0 nm wavelength of (A) $Tm_{0.005}Y_{0.995}NbO_4$ and (B) $Tm_{0.038}Y_{0.962}NbO_4$ powder phosphor in the wavelength range of 275–850 nm are shown in part (2) of Fig. 1. The Tm^{3+}:$YNbO_4$ powder phosphor exhibited four groups of excitation spectra signal peaks between 275 and 850 nm. It is found that their main peaks were positioned at 362.0, 468.0, 682.5, and 789.0 nm. These clearly correspond to the $^3H_6 \rightarrow {}^1D_2$, $^3H_6 \rightarrow {}^1G_4$, $^3H_6 \rightarrow {}^3F_3$, and $^3H_6 \rightarrow {}^3H_4$ absorption transitions, respectively, of the Tm^{3+} ion [12–18].

The visible luminescence spectra of the (A) $Tm_{0.005}Y_{0.995}NbO_4$ and (B) $Tm_{0.038}Y_{0.962}NbO_4$ powder phosphors were then measured. The luminescence spectra at 750–1020 nm, when $^3F_3$ state of the Tm^{3+}:$YNbO_4$ powder phosphor is excited by 682.5 nm light, were measured, as shown in Fig. 2. A medium-sized luminescence peak at (789.0, 802.5 nm) assigned to the $^3H_4 \rightarrow {}^3H_6$ fluorescence for the Tm^{3+}:$YNbO_4$ powder phosphor was observed. The luminescence spectra at 510–850 nm, when $^1G_4$ state of the Tm^{3+}:$YNbO_4$ powder phosphor is excited by 461.0 nm light, were measured, as shown in Fig. 3. In this case, two medium-sized luminescence peaks at 648.0 nm and (791.0, 802.5 nm) of the $^1G_4 \rightarrow {}^3F_4$ and $^3H_4 \rightarrow {}^3H_6$ fluorescence of the Tm^{3+}:$YNbO_4$ powder

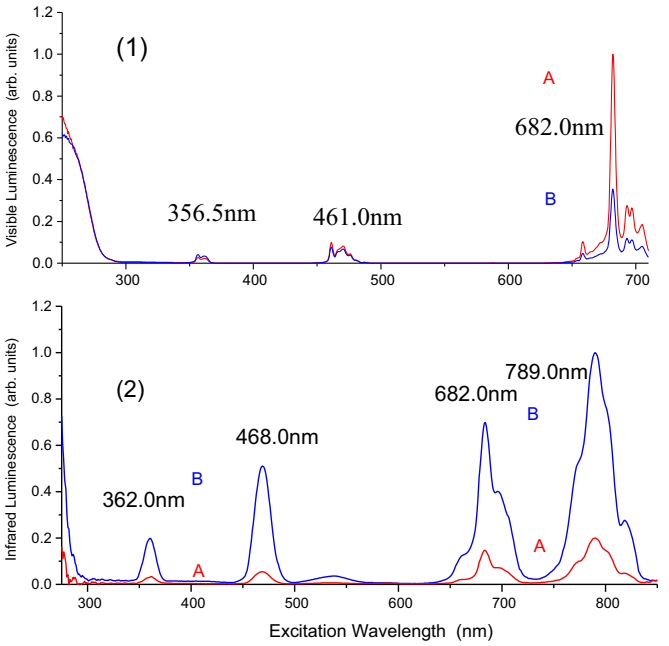

Fig. 1. Visible (1) and infrared (2) excitation spectra of (A) $Tm_{0.005}Y_{0.995}NbO_4$ (red) and (B) $Tm_{0.038}Y_{0.962}NbO_4$ (blue) powder phosphors obtained when the fluorescence received wavelength is positioned at 802.5 nm (1) and 1820.0 nm (2). (For interpretation of the references to color in this figure legend, the reader is referred to the web version of this article.)

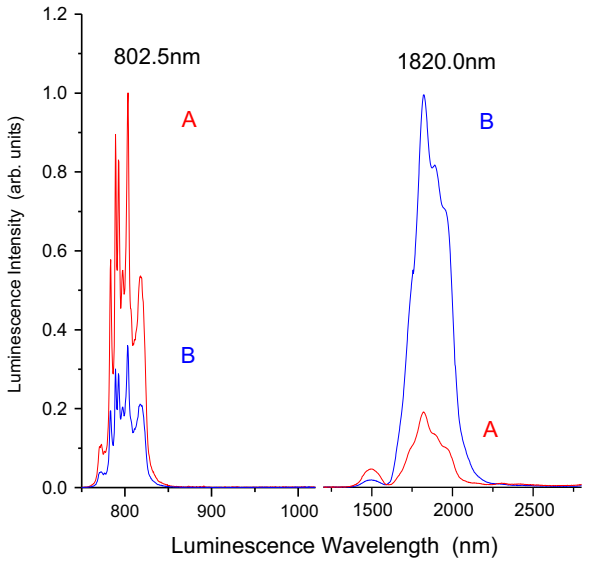

Fig. 2. Luminescence spectra of (A) $Tm_{0.005}Y_{0.995}NbO_4$ (red) and (B) $Tm_{0.038}Y_{0.962}NbO_4$ (blue) powder phosphor obtained when the 682.5 nm $^3H_6 \rightarrow {}^3F_3$ excitation peak was selected as the excitation wavelength. (For interpretation of the references to color in this figure legend, the reader is referred to the web version of this article.)

phosphor were observed. The luminescence spectra at 418–700 and 700–1000 nm, when $^1D_2$ state is excited by 356.5 nm light, were measured. A strong luminescence peak at (452.5, 456.0 nm), a small peak at (656.5, 662.0, 666.5 nm), and a medium-sized peak at (789.0, 802.5 nm) were observed, corresponding to the luminescence transitions of $^1D_2 \rightarrow {}^3F_4$, $^1G_4 \rightarrow {}^3F_4$, and $^3H_4 \rightarrow {}^3H_6$, respectively [12–18]. The luminescence spectra when excited by 356.5 nm are similar to that when excited by 682.5 nm and 461.0 nm light.

The infrared luminescence spectra of the (A) $Tm_{0.005}Y_{0.995}NbO_4$ and (B) $Tm_{0.038}Y_{0.962}NbO_4$ powder phosphors were also measured.

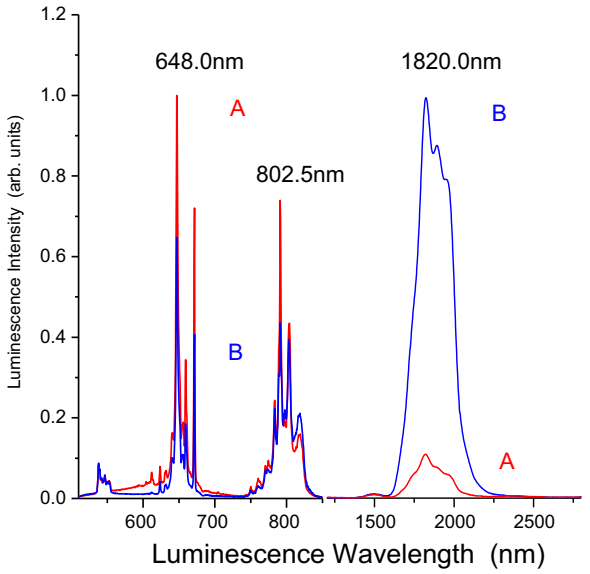

Fig. 3. Luminescence spectra of (A) $Tm_{0.005}Y_{0.995}NbO_4$ (red) and (B) $Tm_{0.038}Y_{0.962}NbO_4$ (blue) powder phosphor obtained when the 461.0 nm (for visible) or 468.0 nm (for infrared) $^3H_6 \rightarrow {}^1G_4$ excitation peak was selected as the excitation wavelength. (For interpretation of the references to color in this figure legend, the reader is referred to the web version of this article.)

In the same manner, the $^3F_3$, $^1G_4$, and $^1D_2$ state of the Tm^{3+}:$YNbO_4$ powder phosphor were also excited by the 682.5, 468.0, and 362.0 nm light to measure the luminescence spectra at 1200–2800 nm, as shown in Figs. 2 and 3. Two groups of luminescence peaks positioned at 1496.0 nm and 1820.0 nm were observed, which are clearly the $^3H_4 \rightarrow {}^3F_4$ and $^3F_4 \rightarrow {}^3H_6$ luminescence transitions [12–18]. It can be seen that the 1820.0 nm $^3F_4 \rightarrow {}^3H_6$ near-infrared luminescence signal intensity of the (B) $Tm_{0.038}Y_{0.962}NbO_4$ powder phosphor is much intense than that of (A) $Tm_{0.005}Y_{0.995}NbO_4$.

The fluorescence lifetimes of the 802.5, 648.0, and 456.0 nm visible fluorescences of the (A) $Tm_{0.005}Y_{0.995}NbO_4$ and (B) $Tm_{0.038}Y_{0.962}NbO_4$ powder phosphors, as shown in Fig. 4, were measured also. The pumping sources for the measurements were a

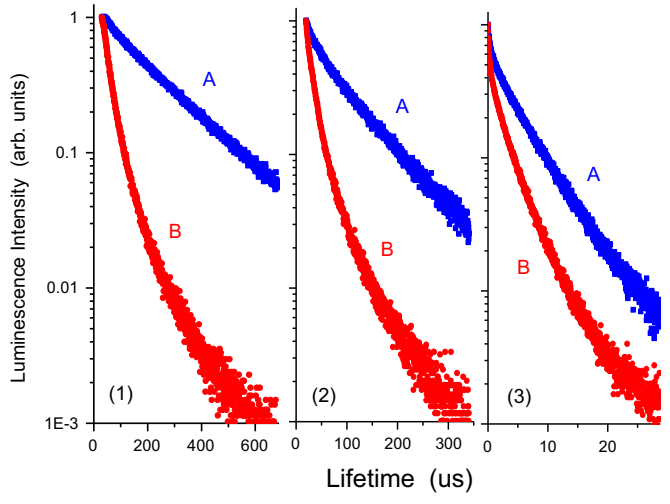

Fig. 4. Fluorescence lifetimes of the (1) 802.5 nm (left), (2) 648.0 nm (middle), and (3) 456.0 nm (right) visible luminescences of (A) $Tm_{0.005}Y_{0.995}NbO_4$ (blue) and (B) $Tm_{0.038}Y_{0.962}NbO_4$ (red) powder phosphors, when excited by (1) 682.5 nm (left), (2) 461.0 nm (middle), and (3) 368.0 nm (right) pulsed light. (For interpretation of the references to color in this figure legend, the reader is referred to the web version of this article.)

360 nm NanoLED semiconductor quasi-laser and pulse Xe lamp. All the fluorescence lifetime values were fitted from the measured fluorescence lifetime experimental curves [1–2,5–8,12,14,15,16,17,19–20,25], using the tail-fit method. The origin points of fit were set after the fluorescence-spectrometer equipment response. From the analysis of measured experimental lifetime curves results, the fluorescence lifetime values of the 802.5, 648.0, and 456.0 nm fluorescences of (A) $Tm_{0.005}Y_{0.995}NbO_4$ were found to be τ_A(802.5 nm)=230.10 μs, τ_A(648.0 nm)=102.68 μs, and τ_A(456.0 nm)=5.7760 μs, respectively; those of (B) $Tm_{0.038}Y_{0.962}NbO_4$ were found to be τ_B(802.5 nm)=79.487 μs; τ_B(648.0 nm)=41.612 μs and τ_B(456.0 nm)=3.4850 μs, respectively.

4. Analysis

It is well-known that the total decay rate W_{tot} of Tm^{3+} ion at 0.5% concentration can be written as following [2]:

$$W_{tot\ Tm(0.5\%)} = A + W_{MP} = \tau^{-1}{}_{Tm(0.5\%)} \tag{1}$$

where A is the spontaneous radiative rate, W_{MP} is the multi-phonon relaxation rate, $\tau_{Tm(0.5\%)}$ is the luminescence lifetime of the Tm^{3+} ion whose concentration is of 0.5%. In formula (1), It is assumed that the energy transfer among the Tm^{3+} ions is very small when x=0.5%, which can represent the case of non-energy transfer. Therefore we have that the total decay rate of Tm^{3+} ion in x% concentration can be given by [2]:

$$W_{tot\ Tm(x\%)} = A + W_{MP} + W_{ET} = \tau^{-1}{}_{Tm(x\%)} \tag{2}$$

where W_{ET} is the energy transfer rate, and $\tau_{Tm(x\%)}$ is the luminescence lifetime of the Tm^{3+} ion in x% concentration. From formulae (1) and (2), we have that the energy transfer efficiency can be given by [2]:

$$\eta_{ET,x\%Tm} = \frac{W_{ET}}{A + W_{MP} + W_{ET}} = 1 - \frac{\tau_{Tm(x\%)}}{\tau_{Tm(0.5\%)}} \tag{3}$$

Meanwhile, according to well-known infrared quantum cutting literature, the energy transfer efficiency of the Tm^{3+} ion caused by cross-relaxation energy transfer can be given by formula (4) also [1–2,5–8,12,14–17,19–20,25]:

$$\eta_{tr,x\%Tm} \approx 1 - \frac{\int I_{x\%Tm}\,dt}{\int I_{0.5\%Tm}\,dt} \tag{4}$$

where I denotes intensity, and x%Tm represents the Tm^{3+} concentration. In fact, we have found that the results calculated from formulae (3) and (4) are very close and near.

Therefore, the energy transfer efficiencies of the 802.5, 648.0, and 456.0 nm fluorescences are calculated from formula (3) to be $\eta_{ET,3.8\%Tm}(802.5nm) = 65.5\%$, $\eta_{ET,3.8\%Tm}(648.0nm) = 59.5\%$, and $\eta_{ET,3.8\%Tm}(456.0nm) = 39.7\%$.

The schematic diagram of energy level structure and quantum cutting process is shown in Fig. 5. It can be seen from Fig. 1 that the intensity of the 802.5 nm excitation spectrum for (B) $Tm_{0.038}Y_{0.962}NbO_4$ powder phosphor is only slightly smaller than that of (A) $Tm_{0.005}Y_{0.995}NbO_4$. However, the intensity of the 1820.0 nm excitation spectrum for (B) $Tm_{0.038}Y_{0.962}NbO_4$ powder phosphor is much larger than that of (A) $Tm_{0.005}Y_{0.995}NbO_4$. The enhancement between the intensity of (B) $Tm_{0.038}Y_{0.962}NbO_4$ and (A) $Tm_{0.005}Y_{0.995}NbO_4$ for 1820.0 nm excitation spectrum is much larger than the reduction for that of 802.5 nm excitation spectrum. It illustrates that the luminescent energy of $^3H_4$ level is transfer into $^3F_4$ level. Moreover, it illustrates that it is the multi-photon process but linear process because one portion reduction in 802.5 nm luminescence intensity results in multi portions

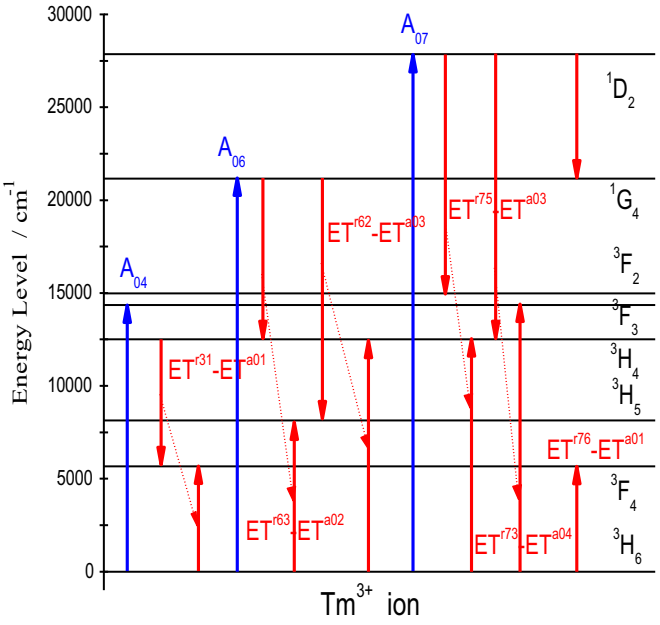

Fig. 5. Schematic diagram of energy level structure and quantum cutting process of Tm^{3+}:$YNbO_4$ powder phosphor. In the figure, "*A*" or "*a*" represents absorption, "ET" represents energy transfer, "*r*" represents release energy. The number 0 to 7 represent the energy level from $^3H_6$ state to $^1D_2$ level. For example, ET^{r76}-ET^{a01} represents $\{^1D_2 \rightarrow {}^1G_4, {}^3H_6 \rightarrow {}^3F_4\}$ cross-energy transfer process.

increment in 1820.0 nm luminescence intensity [1–2,5–8,12,14–17,19–20,25]. Further, it can be seen from luminescence spectra of Figs. 2 and 3 that when the Tm^{3+} ion concentration is enhanced from 0.5% to 3.8%, the infrared 1820.0 nm luminescence intensities are enhanced about 8 to 10 times meanwhile the visible luminescence intensities are reduced only about 2 times. It means that what we have observed is a multi-photon near-infrared quantum cutting luminescence phenomena just as Meijerink et al. point out. It is significant that present observed near-infrared quantum cutting luminescence phenomena is excellent because the 8 to 10 times enhancement in the infrared 1820.0 nm luminescence intensities are much intense than 2 times reduction in visible luminescence intensities. More careful analysis is described at following.

When the $^3H_4$, $^3F_3$, and $^3F_2$ energy levels are excited, many Tm^{3+} ions may be populated at the $^3H_4$ energy level owing to the rapid multiphonon non-radiative relaxation from $^3F_3$ and $^3F_2$ energy levels to $^3H_4$. The Tm^{3+} ion possesses a very effective $\{^3H_4 \rightarrow {}^3F_4, {}^3H_6 \rightarrow {}^3F_4\}$ CR1:ET^{r31}-ET^{a01} cross-energy transfer process. Although its transition mismatch $+858.5\ cm^{-1}$ is large, however the reduced matrix elements $(U^{\lambda})^2$ (0.1275, 0.1311, 0.2113) and (0.5375, 0.7261, 0.2382) of the Tm^{3+} ion are extremely large [12–18] such that the cross energy transfer rate of $\{^3H_4 \rightarrow {}^3F_4, {}^3H_6 \rightarrow {}^3F_4\}$ CR1:ET^{r31}-ET^{a01} is also very large. For (B) $Tm_{0.038}Y_{0.962}NbO_4$ powder phosphor, the population of the $^3H_4$ energy level may directly transfer to the first excited state $^3F_4$ energy level through the $\{^3H_4 \rightarrow {}^3F_4, {}^3H_6 \rightarrow {}^3F_4\}$ CR1:ET^{r31}-ET^{a01} cross-energy transfer process. This results in the very effective two-photon near-infrared quantum cutting of the $^3F_4 \rightarrow {}^3H_6$ fluorescence.

When the $^1G_4$ energy level is excited, many Tm^{3+} ions may populate at the $^1G_4$ energy level because the $^1G_4$ energy level is a metastable energy state. In this case, the Tm^{3+} ion possesses a very effective $\{^1G_4 \rightarrow {}^3H_4, {}^3H_6 \rightarrow {}^3H_5\}$ CR2:ET^{r63}-ET^{a02} cross-energy transfer process. Its transition mismatch $+51.5\ cm^{-1}$ is small, and the reduced matrix elements $(U^{\lambda})^2$ (0.1645, 0.0052, 0.4114) and (0.1074, 0.2314, 0.6385) of Tm^{3+} ion are very large [12–20], so the cross-energy transfer rate of $\{^1G_4 \rightarrow {}^3H_4, {}^3H_6 \rightarrow {}^3H_5\}$ CR2:ET^{r63}-ET^{a02} is very large. The Tm^{3+} ion also possesses a very effective $\{^1G_4 \rightarrow {}^3H_5, {}^3H_6 \rightarrow {}^3H_4\}$ CR8:ET^{r62}-ET^{a03} cross-energy transfer process. Its transition mismatch $+51.5\ cm^{-1}$ is small, and its reduced matrix elements $(U^{\lambda})^2$ (0.0773, 0.0078, 0.5633) and (0.2357, 0.1081, 0.5916) are very large [12–18], so the cross-energy transfer rate of $\{^1G_4 \rightarrow {}^3H_5, {}^3H_6 \rightarrow {}^3H_4\}$ CR8:ET^{r62}-ET^{a03} is very large. Other cross-energy transfer processes are also found to have smaller transfer rates. Therefore, for the (B) $Tm_{0.038}Y_{0.962}NbO_4$ powder phosphor, the population of the $^1G_4$ energy level may directly transfer to the lower energy level mainly through the $\{^1G_4 \rightarrow {}^3H_4, {}^3H_6 \rightarrow {}^3H_5\}$ CR2:ET^{r63}-ET^{a02} and $\{^1G_4 \rightarrow {}^3H_5, {}^3H_6 \rightarrow {}^3H_4\}$ CR8:ET^{r62}-ET^{a03} cross-energy transfer processes, i.e., one population of the $^1G_4$ energy level may very effectively lead to two populations, which are positioned at the $^3H_4$ and $^3H_5$ energy levels, respectively, mainly through the $\{^1G_4 \rightarrow {}^3H_4, {}^3H_6 \rightarrow {}^3H_5\}$ CR2:ET^{r63}-ET^{a02} and $\{^1G_4 \rightarrow {}^3H_5, {}^3H_6 \rightarrow {}^3H_4\}$ CR8:ET^{r62}-ET^{a03} cross-energy transfer processes. This may also very effectively lead to three populations of the $^3F_4$ energy level through the CR1:ET^{r31}-ET^{a01}$\{^3H_4 \rightarrow {}^3F_4, {}^3H_6 \rightarrow {}^3F_4\}$ cross-energy transfer process from the $^3H_4$ level and multi-phonon non-radiative relaxation from the $^3H_5$ level, respectively. This results in the effective three-photon near-infrared quantum cutting of the $^3F_4 \rightarrow {}^3H_6$ fluorescence of Tm^{3+} ion.

When the $^1D_2$ energy level is excited, many Tm^{3+} ions may be populated at the $^1D_2$ energy level because the $^1D_2$ energy level is a metastable energy state. In this case the Tm^{3+} ion possesses an effective $\{^1D_2 \rightarrow {}^1G_4, {}^3H_6 \rightarrow {}^3F_4\}$ CR9:ET^{r76}-ET^{a01} cross-energy transfer process. Although its transition mismatch $+474.5\ cm^{-1}$ is large, however the reduced matrix elements $(U^{\lambda})^2$ (0.1874, 0.1799, 0.0022) and (0.5375, 0.7261, 0.2382) of the Tm^{3+} ion are very large as well [12–20], so the cross-energy transfer rate of $\{^1D_2 \rightarrow {}^1G_4, {}^3H_6 \rightarrow {}^3F_4\}$ CR9:ET^{r76}-ET^{a01} is also large. The Tm^{3+} ion also possesses an effective $\{^1D_2 \rightarrow {}^3F_2, {}^3H_6 \rightarrow {}^3H_4\}$ CR10:ET^{r75}-ET^{a03} cross-energy transfer process. Although its transition mismatch $-219.9\ cm^{-1}$ is large, however the reduced matrix elements $(U^{\lambda})^2$ (0.0643, 0.3065, 0) and (0.2357, 0.1081, 0.5916) of the Tm^{3+} ion are very large [12–18], therefore the cross-energy transfer rate of $\{^1D_2 \rightarrow {}^3F_2, {}^3H_6 \rightarrow {}^3H_4\}$ CR10:ET^{r75}-ET^{a03} is large. The Tm^{3+} ion also possesses an effective $\{^1D_2 \rightarrow {}^3H_4, {}^3H_6 \rightarrow {}^3F_3\}$ CR12:ET^{r73}-ET^{a04} cross-energy transfer process. Its transition mismatch $+388.9\ cm^{-1}$ is large, and however its reduced matrix elements $(U^{\lambda})^2$ (0.1248, 0.0096, 0.2280) and (0, 0.3164, 0.8413) of Tm^{3+} ion are very large [12–20], so the cross-energy transfer rate of $\{^1D_2 \rightarrow {}^3H_4, {}^3H_6 \rightarrow {}^3F_3\}$ CR12:ET^{r73}-ET^{a04} is also large. The other cross-energy transfer processes are found to have smaller transfer rates. Therefore, for (B) $Tm_{0.038}Y_{0.962}NbO_4$ powder phosphor, the population of the $^1D_2$ energy level may directly transfer to the lower energy level mainly through the $\{^1D_2 \rightarrow {}^3F_2, {}^3H_6 \rightarrow {}^3H_4\}$ CR10:ET^{r75}-ET^{a03}, $\{^1D_2 \rightarrow {}^3H_4, {}^3H_6 \rightarrow {}^3F_3\}$ CR12:ET^{r73}-ET^{a04} and $\{^1D_2 \rightarrow {}^1G_4, {}^3H_6 \rightarrow {}^3F_4\}$ CR9:ET^{r76}-ET^{a01} cross-energy transfer processes. For CR10:ET^{r75}-ET^{a03} and CR12:ET^{r73}-ET^{a04}, one population of the $^1D_2$ energy level may very effectively lead to two populations of the $^3H_4$ energy level. For CR9:ET^{r76}-ET^{a01}, one population of the $^1D_2$ energy level may very effectively lead to two populations positioned at the $^1G_4$ and $^3F_4$ energy levels. They may also effectively lead to four populations of the $^3F_4$ energy level as a consequence. This process results in the effective four-photon near-infrared quantum cutting of the $^3F_4 \rightarrow {}^3H_6$ fluorescence of the Tm^{3+} ion.

Therefore, the up-limit of two-photon, three-photon, and four-photon near-infrared quantum cutting efficiency of the 1820.0 nm $^3F_4 \rightarrow {}^3H_6$ fluorescence when the $^3F_3$, $^1G_4$, and $^1D_2$ energy levels are excited by 682.5 nm, 461.0 nm, and 362.0 nm light, respectively, can be expressed using formulae (5a) and (5b) for two-photon, (6a) and (6b) for three-photon, (7a) and (7b) for four-photon of

CR9:ET^{r76}-ET^{a01}, and (8a) and (8b) for four-photon of CR10:ET^{r75}-ET^{a03} and CR12:ET^{r73}-ET^{a04} on best standard condition [1–2,5–8,12,14–17,19–20,25]:

$$\eta_{CR,x\%Tm}\left({}^3H_4\right) = \eta_{{}^3H_4}\bullet\left[1-\eta_{ET,x\%Tm}\left({}^3H_4\right)\right] + \left(1-\eta_{{}^3H_4}\right)\bullet\eta_{lower}\bullet\left[1-\eta_{ET,x\%Tm}\left({}^3H_4\right)\right] + 2\eta_{{}^3F_4}\eta_{ET,x\%Tm}\left({}^3H_4\right) \quad (5a)$$

$$\eta_{CR,x\%Tm}\left({}^3H_4\right)^{UL} = 1+\eta_{ET,x\%Tm}\left({}^3H_4\right) \quad (5b)$$

In formula (5a) and (5b), $\eta_{{}^3F_4}\eta_{ET,x\%Tm}({}^3H_4)$ is the efficiency of population from $^3H_4$ to $^3F_4$ induced by cross-energy transfer. $\eta_{{}^3H_4}\bullet[1-\eta_{ET,x\%Tm}({}^3H_4)]$ is the luminescence efficiency of the population remained in $^3H_4$ state. $(1-\eta_{{}^3H_4})\bullet\eta_{lower}\bullet[1-\eta_{ET,x\%Tm}({}^3H_4)]$ is the efficiency of population luminescent in lower level after they is from $^3H_4$ to lower level induced by multi-phonon non-radiative relaxation.

$$\eta_{CR,x\%Tm}\left({}^1G_4\right) = \eta_{{}^1G_4}\bullet\left[1-\eta_{ET,x\%Tm}\left({}^1G_4\right)\right] + \left\{\left(1-\eta_{{}^1G_4}\right)\bullet\eta_{lower}\bullet\left[1-\eta_{ET,x\%Tm}\left({}^1G_4\right)\right] + \eta_{{}^3H_4}\eta_{ET,x\%Tm}\left({}^1G_4\right)\right\}\bullet\left\{\eta_{CR,x\%Tm}\left({}^3H_4\right)\right\} + \eta_{{}^3F_4}\eta_{ET,x\%Tm}\left({}^1G_4\right) \quad (6a)$$

$$\eta_{CR,x\%Tm}\left({}^1G_4\right)^{UL} = 1+\eta_{ET,x\%Tm}\left({}^1G_4\right) + \eta_{ET,x\%Tm}\left({}^1G_4\right)\bullet\eta_{ET,x\%Tm}\left({}^3H_4\right) \quad (6b)$$

$$\eta_{CR,x\%Tm}\left({}^1D_2\right) = \eta_{{}^1D_2}\bullet\left[1-\eta_{ET,x\%Tm}\left({}^1D_2\right)\right] + \left\{\left(1-\eta_{{}^1D_2}\right)\bullet\eta_{lower}\bullet\left[1-\eta_{ET,x\%Tm}\left({}^1D_2\right)\right] + \eta_{{}^1G_4}\eta_{ET,x\%Tm}\left({}^1D_2\right)\right\}\bullet\left\{\eta_{CR,x\%Tm}\left({}^1G_4\right)\right\} + \eta_{{}^3F_4}\eta_{ET,x\%Tm}\left({}^1D_2\right) \quad (7a)$$

$$\eta_{CR,x\%Tm}\left({}^1D_2\right)^{UL} = 1+\eta_{ET,x\%Tm}\left({}^1D_2\right)+\eta_{ET,x\%Tm}\left({}^1D_2\right)\bullet\eta_{ET,x\%Tm}\left({}^1G_4\right) + \eta_{ET,x\%Tm}\left({}^1D_2\right)\bullet\eta_{ET,x\%Tm}\left({}^1G_4\right)\bullet\eta_{ET,x\%Tm}\left({}^3H_4\right) \quad (7b)$$

$$\eta_{CR,x\%Tm}\left({}^1D_2\right) = \eta_{{}^1D_2}\bullet\left[1-\eta_{ET,x\%Tm}\left({}^1D_2\right)\right]+\left\{\left(1-\eta_{{}^1D_2}\right)\bullet\eta_{lower}\bullet\left[1-\eta_{ET,x\%Tm}\left({}^1D_2\right)\right] + \eta_{{}^3H_4}\eta_{ET,x\%Tm}\left({}^1D_2\right)\right\}\bullet\left\{\eta_{CR,x\%Tm}\left({}^3H_4\right)\right\} + \eta_{{}^3H_4}\eta_{ET,x\%Tm}\left({}^1D_2\right)\bullet\left\{\eta_{CR,x\%Tm}\left({}^3H_4\right)\right\} \quad (8a)$$

$$\eta_{CR,x\%Tm}\left({}^1D_2\right)^{UL} = 1+\eta_{ET,x\%Tm}\left({}^1D_2\right) + 2\bullet\eta_{Et,x\%Tm}\left({}^1D_2\right)\bullet\eta_{ET,x\%Tm}\left({}^3H_4\right) \quad (8b)$$

where $\eta_{CR,x\%Tm}({}^3H_4)$ of (5a) and (5b), $\eta_{CR,x\%Tm}({}^1G_4)$ of (6a) and (6b), and $\eta_{CR,x\%Tm}({}^1D_2)$ of (7a)–(8b) are the two-photon, three-photon, and four-photon near-infrared quantum cutting efficiency of the {CR1:ET^{r31}-ET^{a01}} of (5a) and (5b), { CR2:ET^{r63}-ET^{a02} and CR8:ET^{r62}-ET^{a03}} of (6a) and (6b), CR9:ET^{r76}-ET^{a01} of (7a) and (7b), and {CR10:ET^{r75}-ET^{a03}, CR12:ET^{r73}-ET^{a04} } cross-energy transfers of (8a) and (8b), respectively. $\eta_{ET,x\%Tm}({}^3H_4)$, $\eta_{ET,x\%Tm}({}^1G_4)$, and $\eta_{ET,x\%Tm}({}^1D_2)$ are the respective energy transfer efficiencies. And $\eta_{{}^1D_2}$, $\eta_{{}^1G_4}$, $\eta_{{}^3H_4}$, and $\eta_{{}^3F_4}$ and η_{lower} are the luminescent efficiencies of the $^1D_2$, $^1G_4$, $^3H_4$, and $^3F_4$ and lower energy levels of the Tm^{3+} ion, respectively. We assume that $\eta_{{}^1D_2}=\eta_{{}^1G_4}=\eta_{{}^3H_4}=\eta_{{}^3F_4}=\eta_{lower}=1$, as is also assumed in most near-infrared quantum cutting literature [1–2,5–8,12,14–17,19–20,25]. Therefore, from (5a) and (5b), $\eta_{CR,3.8\%Tm}({}^3H_4)^{UL}=\eta_{CR,3.8\%Tm}(682.5\ nm)^{UL}=165.5\%$. Secondly, from (6a) and (6b) $\eta_{CR,3.8\%Tm}({}^1G_4)^{UL}=\eta_{CR,3.8\%Tm}(461.0\ nm)^{UL}=198.5\%$. From (7a) and (7b), $\eta_{CR,3.8\%Tm}({}^1D_2)^{UL}=\eta_{CR,3.8\%Tm}(362.0\ nm)^{UL}=178.8\%$. Finally, from (8a) and (8b), $\eta_{CR,3.8\%Tm}({}^1D_2)^{UL}=\eta_{CR,3.8\%Tm}(362.0\ nm)^{UL}=191.7\%$.

These analyses about the quantum cutting efficiency and mechanism are coincided with the experiment measured results. It is needed also to point out that the action of the phonon equal to 0 is not the most largest point for near infrared quantum cutting luminescence of Tm^{3+} ion. The most largest point for near infrared quantum cutting luminescence of Tm^{3+} ion would be positioned at the field which has a slight phonon action. Because quantum cutting needs higher doping concentration of rare earth ion, in order to achieve intense cross energy transfer and further to achieve intense near infrared quantum cutting luminescence. However, the actual material is difficult to possess the ideal condition of entire resonance for all energy transfer. It is excellent enough for that all energy transfers are all near entire resonant. Therefore it is needed a slight assistant action of phonon to achieve effective intense phonon-assistant energy transfers.

5. Conclusion

In conclusion, two-photon, three-photon, and four photon near-infrared quantum cutting luminescence of Tm^{3+} activator in $YNbO_4$ powder phosphor is reported in present study. The two-photon, three-photon, and four-photon quantum cutting mechanism, induced by various energy transfer processes, are analyzed carefully. The largest up-limit of the two-, three-, and four-photons near-infrared quantum cutting efficiencies are found to be approximately 166%, 198%, and 192%, respectively.

Acknowledgment

Project is supported by the National Natural Science Foundation of China (51472028) and the significant project of Fundamental Research Funds for the Central Universities of China (212-105560GK). The author thanks very much for the help of Academician Prof. Jingkui Liang, Academician Prof. Guoqiang Ni, Prof. Kexin Chen, Dr. Yu Ye, Prof. Jinguang Wu, Prof. Zhiyong Tang, Prof. Sijie Gao, Engineer Rui Guo, Prof. Anru Lou, Prof. Jian Zhuang, Prof. Liwei Zhou, Prof. Lin Zhai.

References

[1] P. Vergeer, T.J.H. Vlugt, M.H.F. Kox, M.I. den Hertog, J.P.J.M. van der Eerden, A. Meijerink, Phys. Rev. B 71 (1) (2005) 014119.
[2] J.J. Zhou, Y. Teng, X.F. Liu, S. Ye, Z.J. Ma, J.R. Qiu, Phys. Chem. Chem. Phys. 12 (41) (2010) 13759–13762.
[3] R.T. Wegh, H. Donker, K.D. Oskam, A. Meijerink, Science 283 (54 02) (1999) 663–666.
[4] B.S. Richards, Sol. Energy Mater. Sol. Cells 90 (9) (2006) 1189–1207.
[5] W.J. Zhu, D.Q. Chen, L. Lei, J. Xu, Y.S. Wang, Nanoscale 6 (18) (2014) 10500–10504.
[6] D.Q. Chen, Y.S. Wang, M.C. Hong, Nano Energy 1 (1) (2012) 73–90.

[7] X.P. Chen, W.J. Zhang, Q.Y. Zhang, Phys. B-Condens. Matter 406 (6-7) (2011) 1248–1252.
[8] X.B. Chen, G.J. Salamo, G.J. Yang, Y.L. Li, X.L. Ding, Y. Gao, Q.L. Liu, J.H. Guo, Opt. Express 21 (18) (2013) A829–A840.
[9] J.Y. Sun, W. Zhou, Y.N. Sun, J.H. Zeng, Opt. Commun. 296 (2013) 84–86.
[10] T. Trupke, M.A. Green, P. Wurfel, J. Appl. Phys. 92 (3) (2002) 1668–1674.
[11] J.D. Chen, H. Guo, Z.Q. Li, H. Zhang, Y.X. Zhuang, Opt. Mater. 32 (9) (2010) 998–1001.
[12] J.J. Zhou, Y. Teng, X.F. Liu, S. Ye, X.Q. Xu, Z.J. Ma, J.R. Qiu, Opt. Express 18 (21) (2010) 21663–21668.
[13] R. Reisfeld, Lasers and Excited States of Rare-Earth, Springer-Verlag, Berlin, 1977.
[14] Y.Z. Wang, D.C. Yu, H.H. Lin, S. Ye, M.Y. Peng, Q.Y. Zhang, J. Appl. Phys. 114 (20) (2013) 203510.
[15] B.M. van der Ende, L. Aarts, A. Meijerink, Phys. Chem. Chem. Phys. 11 (47) (2009) 11081–11095.
[16] Z. Pan, G. Sekar, R. Akrobetu, R. Mu, S.H. Morgan, J. Non-Cryst. Solids 358 (15) (2012) 1814–1817.
[17] M.M. Smedskjaer, J.R. Qiu, J. Wang, Y.Z. Yue, Appl. Phys. Lett. 98 (7) (2011) 071911.
[18] Z.F. Song, Principle and Application of Atomic Spectroscopy and Crystal Spectroscopy, Science Press, Beijing, 1987 (in Chinese).
[19] F.T. Rabouw, A. Meijerink, J. Phys. Chem. C 119 (5) (2015) 2364–2370.
[20] D.H. Li, Y.J. Chen, J.H. Huang, X.H. Gong, Y.F. Lin, Z.D. Luo, Y.D. Huang, Phys. B-Condens. Matter 446 (2014) 12–16.
[21] L. Aarts, S. Jaeqx, B.M. van der Ende, A. Meijerink, J. Lumin. 131 (4) (2011) 608–613.
[22] W.T. Yao, X.B. Chen, H.L. Cheng, G. Zhou, Z.W. Deng, Y.L. Li, D.D. Yan, F.L. Peng, Spectrosc. Spectr. Anal. 35 (2) (2015) 325–328.
[23] K.M. Deng, T. Gong, L.X. Hu, X.T. Wei, Y.H. Chen, M. Yin, Opt. Express 19 (3) (2011) 1749–1754.
[24] D.L. Dexter, Phys. Rev. 108 (3) (1957) 630–633.
[25] X.B. Chen, J.G. Wu, X.L. Xu, Y.Z. Zhang, N. Sawanobori, C.L. Zhang, Q.H. Pan, G. J. Salamo, Opt. Lett. 34 (7) (2009) 887–889.